Electric Vehicle Battery Cooling via Loop Heat Pipes coupled with Underbody Aerodynamics

Marco Bernagozzi[1*], Marco Marengo[2], and Anastasios Georgoulas[1]

[1] *School of Architecture, Technology and Engineering, University of Brighton, Brighton, United Kingdom*
[2] *Department of Civil Engineering and Architecture, University of Pavia, Pavia, Italy*
**Corresponding author email address: m.bernagozzi3@brighton.ac.uk*

Abstract

This paper presents a feasibility study on a fully passive cooling system for electric vehicles using Loop Heat Pipes (LHP) to transfer the batteries excess heat to the underbody of the vehicle. Multiple LHPs are in contact with a battery module, on the evaporator side, while their condensers are embedded in the underbody of the vehicle, cooled via aerodynamic cooling. The study is conducted numerically, by means of a previously validated transient 1-D Lumped Parameter Model (LPM) able to simulate the thermos-fluidic behavior of the LHP, and aerodynamic CFD simulations coupled with heat transfer. The CFD results provide the convection heat transfer coefficient at the condenser wall, which is inputted into the 1-D LPM to design the condenser in order to achieve successful operation of the cooling system, and to evaluate the temperature evolution of the cells. The performance of the proposed cooling system was evaluated over 1C, 2C, 3C charging cycles followed by a 30 minutes 1C driving section. The proposed cooling system was able to contain the cell temperature inside the acceptable limits, even at challenging conditions such as 3C charging, with maximum temperature being 51.6 °C for 3C, 39.3 °C for 2C and 27.5 °C for 1C. All without using any additional energy.

Keywords: Loop Heat Pipe; Electric Vehicle; Aerodynamic Cooling.

1. Introduction

Growing demand for cleaner air and sustainable future, together with a global effort to reduce GreenHouse Gas (GHG) emissions, have pushed the development and adoption of Electric Vehicles (EVs) as the selected choice for passenger transport. EVs numbers are in constant growth, albeit far from the ambitious targets set by several governments worldwide [1]. Reasons are to be found in perceived lack of range, lack of infrastructure, high cost and charging times, amongst others [2].

In order to improve on this limited numbers situation, appropriate thermal management can help tackling problems such as slow charging, lack of range and high cost, as temperature play a critical role on the operation of the batteries. In fact, Li-Ion batteries (the go-to choice for EVs nowadays) desire to be in the narrow range of 25 °C – 40 °C, even if up to 50°C is considered acceptable [3], and to be outside of this range would lead to a reduction in power output and operational life, as well as safety risks, e.g. thermal runaway[4]. In fact, a safety threshold has been set at 60 °C, to avoid the onset of disruptive failure scenarios.

Currently, the most common Battery Thermal Management Systems (BTMS) utilise air or liquid convection. Air convection is preferred when cost and weight are to be minimized, at the expense of performance (e.g. Nissan Leaf, Renault Zoe). This BTMS is simple and cheap but inefficient due to the poor thermal properties of air, and as such it does not allow fast charging. Moreover, it consumes high parasitic power due to the frequent presence of fans [5]. Liquid BTMS, on the other hand, is very efficient and allows for fast charging. It often uses a cold plate at the bottom of the battery pack, or meandering pipes (Tesla), where liquid is moved by a pump [6]. This solution, albeit efficient, is expensive, complex and costly in terms of money and parasitic power.

Research have suggested the use of passive cooling methods, in the forms of PCM, heat pipes and immersion cooling, all with their relative pros and cons. The Authors proposed an innovative BTMS using Loop Heat Pipes and graphite sheets [7], which proved to be successful and allowing better performance than an analogue BTMS relying on active cold plate. In fact, the LHP BTMS was able to reduce the maximum temperature of the cells, compared to the active cold plate BTMS, by 3.6 °C during 10-minutes fast charge at 4C. The LHPs were placed at the bottom of the battery module, acting as thermal vectors between the pack and the HVAC chiller already included in the vehicle, hence reducing the required complexity of the system. More importantly, heat was transferred without the need of parasitic power for the pump. In this scenario, the condenser of the LHP was foreseen to be embedded in the heat exchanger of the HVAC system of the car, hence actively cooled.

In the present work, the Authors propose a variation on the previously developed and tested LHP BTMS, where the condenser is placed on the underbody of the vehicle (as illustrated in Figure 1), cooled by the external ambient air, thus further reducing the parasitic power needed. In this way, aerodynamic cooling of the battery cells is achieved without reducing the aerodynamic performances by increasing the drag (by creating any openings on the exterior of the car).

Figure 1. Idea of the proposed BTMS, where the condenser of the LHP is cooled by aerodynamic forced convection (image modified from ImageFX).

The feasibility of this design is studied numerically, with an experimentally validated 1-D Lumped Parameter Model (LPM) developed by the Authors [8]. This 1-D code is used to calculate the battery cells and LHP evaporator and condenser temperature trends in response to different usage conditions of the batteries (i.e., different driving speeds). In turn, via CFD simulations of the entire vehicle in OpenFOAM CFD Toolbox, a precise estimation of the air temperatures in the vicinity of the vehicle underbody is conducted, leading to the appropriate valued of Heat Transfer Coefficient (HTC) to feed back to the 1-D LPM for the design and evaluation of the condenser feasibility, as well as the prediction of the cells temperature at different charging cycles.

2. Method

The present work utilities two numerical simulations on open-source software coupled together. Firstly, CFD simulations running on OpenFOAM are employed to calculate the heat transfer coefficient (HTC) at the boundary region of the underbody of the car, where the LHP condenser is placed and is rejecting heat to the environment. Secondly, these HTC values are fed back to the 1-D LPM running on Octave, which simulates the excess heat from the cell absorbed by the LHPs, returning the temperature trends of the battery cells. With this method, it is possible to evaluate the effect of different airstream velocities on the thermal performance of the cooling system and design an adequate condenser for different conditions.

2.1. Lumped Parameter Model

In this model, graphite sheets are sandwiched between the battery cells, to improve the heat transfer in the vertical direction, and isolating the cells from one another, ultimately delaying the spreading of an adverse thermal event (e.g., thermal runaway), as shown in Figure 2. The LHP is a flat LHP made out of copper, more details on its geometry can be found on [7]. The working fluid used for the LHP in this case is ethanol.

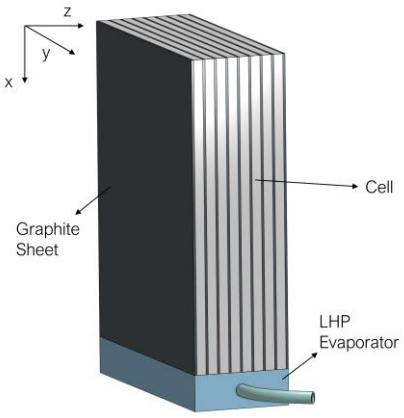

Figure 2. Schematic of the LHP-BTMS with graphite sheets [8].

The proposed Battery Thermal Management Systems uses series of LHPs at the bottom of battery modules. Previous research from the Authors [8] have suggested that a number of LHP evaporators from 2 to 6 can suffice to meet industry requirements, albeit to different standard commiserated with the increased annexed weight. In order to model the thermal behavior of the cell and battery assembly, the thermal network depicted in Figure 3 is used.

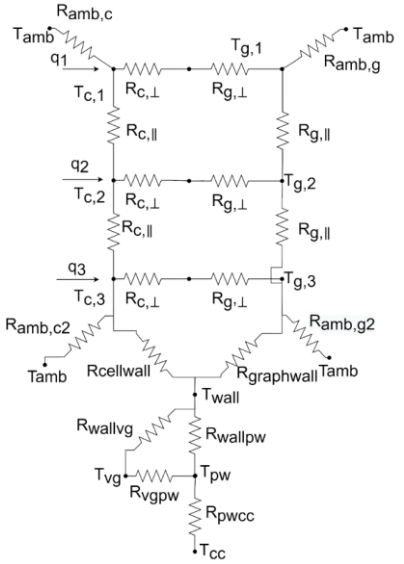

Figure 3. Thermal network used to model the cell, graphite and evaporator assembly.

In this work, the thermal network proposed in Figure 3 is not altered, and its equations and assumptions can be found in previous works of the Authors [8]. Instead, from the previous version of this code, the condenser model was changed to accommodate air convection thermal resistance R_{free}, as shown below:

$$T_{cond,i} = f_{sat}(P_{cond,i}) \quad (1)$$

$$\dot{Q}_{cond,i} = \frac{T_{air} - T_{cond,i}}{R_{air} + R_P + R_{cond}} = \dot{m}(h_{i+1} - h_i) \quad (2)$$

$$h_{i+1} = \frac{\dot{Q}_{cond,i}}{\dot{m}} + h_i \quad (3)$$

$$h_{v,l} = f_{sat}(T_{cond,i}) \quad (4)$$

$$x_{i+1} = f_{sat}(h_{i+1}) = \frac{h_{i+1} - h_l}{h_v - h_l} \quad (5)$$

Eq (1) calculates the internal two-phase fluid temperature, from the assumption of saturated fluid. Eq. (2) calculates the heat lost from the fluid to the air at the i-th node of the condenser, considering three resistances connected in series, i.e., external air convection (heat transfer coefficient h_{air} calculated via CFD simulations), conduction through the pipe and two-phase convection inside the pipe (heat transfer coefficient h_{2p} calculated thanks to Shah correlation).

R_{air}	R_{cond}	R_p
$\frac{1}{h_{air}A_{free}}$	$\frac{1}{h_{2p}A_{cond}}$	$\frac{ln\left(\frac{r_{cond,e}}{r_{cond,i}}\right)}{2\pi k_c L_x}$

Eq (3) calculates the variation in enthalpy due to the loss of power, which then, thanks to the estimation of the vapour enthalpy (eq. 4) from saturation tables, allows to calculate the vapour quality variation (eq 5). Hence, with this algorithm the length of condenser pipe is calculated and checked that it is sufficient to dissipate the amount of heat absorbed at the evaporator, by fully condensing the vapour. A non-complete condensation phenomenon, in the long run, will offset the evaporator-condensation fluid charge balance of the LHP device and eventually lead to dry-out.

This model has been validated for different geometries (cylindrical and flat evaporator) and for different working fluids (water, ethanol, acetone and Novec649) [8].

2.2. CFD Model

For the CFD simulations the open source CFD Toolbox OpenFOAM v. 8.0 was utilised to compute the aerodynamics and the resulting heat transfer distribution in the underbody of the car so that an accurate estimation of the local HTCs could be obtained. In more detail, the buoyantSimpleFoam solver was employed for this purpose.

The mass, momentum, and energy conservation equations govern the fluid movement and interactions. In the considered steady-state turbulent flows, the first two equations, respectively, can be written as follows:

$$\nabla \cdot (\rho u) = 0 \quad (6)$$

$$\frac{\partial(\rho u)}{\partial t} + \nabla \cdot (\rho u u) = -\nabla p + \rho g + \nabla \cdot \left(2\mu_{eff} D(u)\right) - \nabla\left(\frac{2}{3}\mu_{eff}(\nabla \cdot u)\right) \quad (7)$$

Where $\boldsymbol{u}$ is the velocity field, ρ is the density, p is the static pressure, and $\boldsymbol{g}$ is the gravitational acceleration. The effective viscosity μ_{eff} is the sum of turbulent μ_t and dynamic viscosity μ, and $D(\boldsymbol{u})$ is the rate of deformation tensor, defined as:

$$D(u) = \frac{1}{2}(\nabla u + (\nabla u)^T) \quad (8)$$

OpenFOAM determines the pressure gradient and gravity force terms in Equation (7) utilising equation (9) below:

$$-\nabla p + \rho g = -\nabla(p_{rgh} + \rho g \cdot r) + \rho g = -\nabla p_{rgh} - (g \cdot r)\nabla\rho - \rho g + \rho g = -\nabla p_{rgh} - (g \cdot r)\nabla\rho \quad (9)$$

where p_{rgh} is the hydrostatic pressure, $p_{rgh} = p - \rho \boldsymbol{g} \cdot \boldsymbol{r}$, and $\boldsymbol{r}$ is the position vector.

Simulation of heat transfer is performed by solving the energy equation and particularly utilising the sensible enthalpy model of the proposed solver, which solves the following equation (10):

$$\nabla \cdot (\rho u h) + \frac{\partial(\rho K)}{\partial t} + \nabla \cdot (\rho u K) - \frac{dp}{dt} = \nabla \cdot \left(2a_{eff}\nabla h\right) + \rho u \cdot g \quad (10)$$

The enthalpy per unit mass h is the sum of energy per unit mass e and kinematic pressure, $h = e + p/\rho$. $K \equiv |\boldsymbol{u}|^2/2$ is the kinetic energy per unit mass, and α_{eff}/ρ is the effective thermal

diffusivity. For turbulence the standard K-ε model is employed.

3. Results

3.1. CFD Results for HTC estimation

3D symmetric Reynolds Averaged Navier Stokes (RANS) simulations were performed for the purposes of the present investigation. The computational domain and applied boundary conditions are depicted as well as some details of the Computational Mesh are shown in Figure 4.

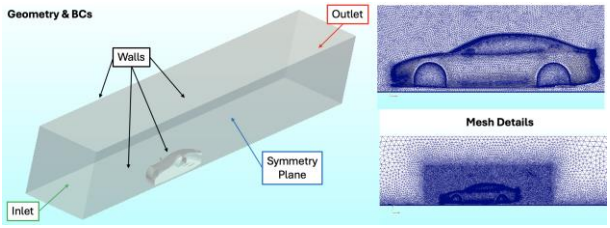

Figure 4. Computational domain, applied boundary conditions and computational mesh details.

As it can be seen from Figure 4, a hybrid, unstructured computational mesh was utilised, consisting of a combination of 8,096,459 tetrahedral and 984,614 prismatic cells. Two types of wall boundaries are employed in the underbody section: a heated wall with a constant temperature condition, which corresponds to a dedicated condenser area for the LHPs; and an adiabatic wall, which corresponds to the remaining outer surface of the considered vehicle underbody. A ~1 m^2 wide surface representing the area occupied by the LHP condenser was superimposed at the underbody of the vehicle and fixed at 40 °C, representing a worse case scenario.

Figure 5 shows the spatial distribution of pressure, velocity and temperature in the vicinity of the vehicle for a speed of 7 m/s (~ 25 km/h). it is evident how the temperature increases towards the end of the area occupied by the condenser, due to the heat received Moreover, top left part of Figure 5 illustrates the sampling plane and line (both located 1 cm below the underbody surface) together with the computed temperature distribution. It is evident how the air temperature increases towards the end of the area occupied by the condenser, due to the heat received by the hot surface. From the top right image of Figure 5 it is evident however how thin is the thermal boundary layer developed by placing the condenser at the underbody.

The horizontal plane positioned 1 cm below the underbody surface helps to visualise the temperature distribution and a sampling line running along the same plane and corresponding to the middle longitudinal axis of the condenser area is used to estimate the local HTCs. The resulting HTCs along the proposed sampling line for the different simulated vehicle speeds, with a total heat emitted from the battery pack of 480 W, are plotted in Figure 6.

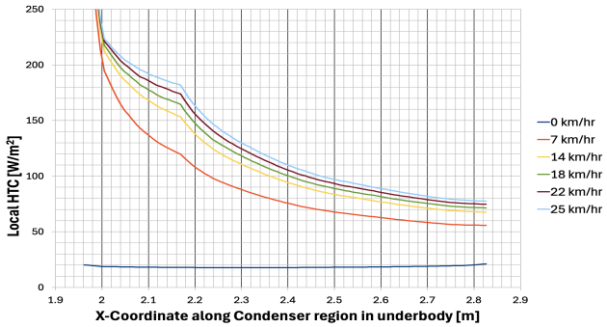

Figure 6. CFD predicted local HTC values versus vehicle moving speed, along the LHP condenser region in the considered vehicle underbody.

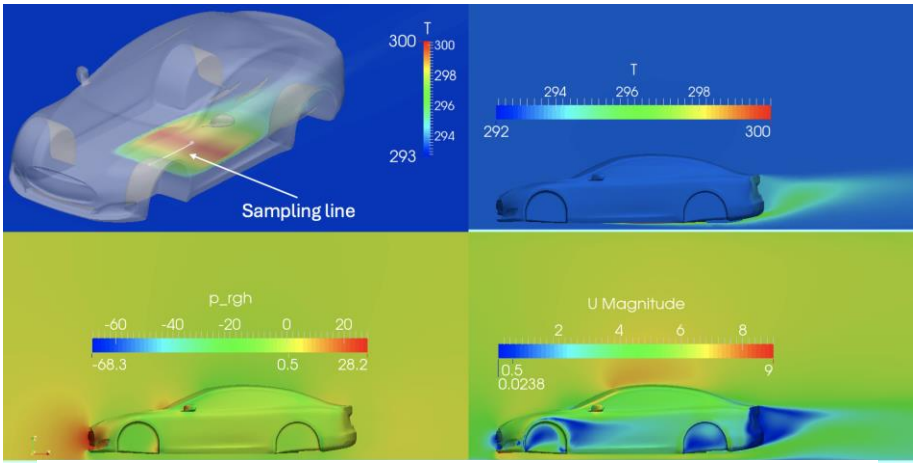

Figure 5. Temperature, pressure and velocity distribution in the vicinity of considered vehicle and sampling line locations for local HTC estimation.

3.2.LPM Results on Cell Temperature

Thanks to the CFD results, now different HTC values are available to be fed back to the LPM code, in order to evaluate the performance of the proposed BTMS, using LHPs, graphite sheets and aerodynamic forced convection at the LHP condenser.

In order to replicate scenarios representative of a real situation, it was chosen to simulate a charging break undertaken by the vehicle, followed by a 30-minute period of driving at 25 km/h (7 m/s). The C-Rate selected were 1C, 2C and 3C, with the last one representing the state of the art in terms of fast charging. The C-Rate is a measure of the rate at which a battery is discharged or charged, relative to its maximum capacity; in fact, it is defined as the discharging/charging current divided by the battery capacity, e.g., 1C means full charge in one hour, 0.5C full charge in 2 hours and so on. Charging the batteries from 20% to 80% capacity at these currents would take 36, 18 and 12 minutes, respectively.

Figure 7 shows the trends of the heating power emitted by a single cell during these three scenarios. The time average values for these cycles are 3 W for 1C, 12 W for 2C and 27 W for 3C. The assumed pack architecture is composed by 8 modules made by 12 cells each, hence the heating powers released by the pack in the three cases are 288 W for 1C, 1152 W for 2C and 2592 W for 3C. It is evident how there is significant difference between different usages, which makes the design of these systems quite challenging.

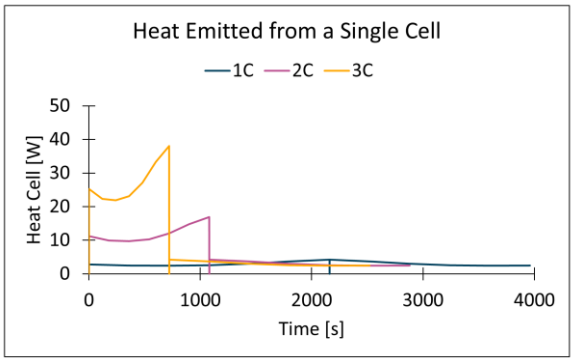

Figure 7. Plot showing the different trends of heat release by a single cell during the different cycles.

A notable aspect of these cycles is that they extend beyond the charging phase, which is often the sole focus in the literature. Instead, they encompass the post-charging period, evaluating the BTMS ability to maintain cells temperatures within acceptable parameters.

Using the temperature values resulting from the CFD simulations, it is possible to estimate the HTC at different velocities. In this case it is of interest to look at the values for 0 and 7 m/s. Because in the CFD model it was assume a worst-case scenario of constant condenser temperature of 40 °C, by changing the heat released at the underbody one can calculate the HTC related to the different charging phases, as shown in Table 1.

Table 1. HTC (in W/m^{2}K) at different charging phases and different speeds (in m/s) calculated from the temperature variations obtained by the CFD simulations.

Speed (m/s)	1C	2C	3C
0	11	44	99
2	59	237	534
4	71	285	641
5	75	300	675
6	78	313	703
7	81	323	727

As previously mentioned, in this paper only the velocity of 0 m/s (charging phase, stationary vehicle) and 7 m/s (urban driving vehicle) are considered. Higher velocities will be considered in future stages of this work.

After several iterations, a solution was found that would ensure full condensation of the working fluid inside the LHP condenser. As a result, suitable geometrical parameters were selected, presented in Table 2.

Table 2. Selected geometrical parameters for LHP condenser design.

#LHP	4	
L cond	2.5	m
ID/OD	6/6.5	mm

Furthermore, simulations results indicated that 4 LHPs (Figure 8) applied to the battery module provide superior performance compared to 2 LHPs, as proved by the results of the average cell temperature shown in Figure 9, where for 2 LHPs the safety threshold of 60 °C is exceeded.

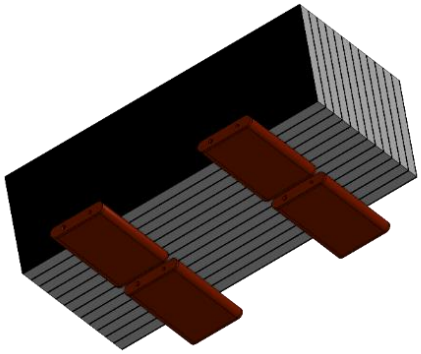

Figure 8. 12-cell module cooled down by 4 LHP evaporators. Piping coming in and out of the evaporator were omitted from the image for clarity.

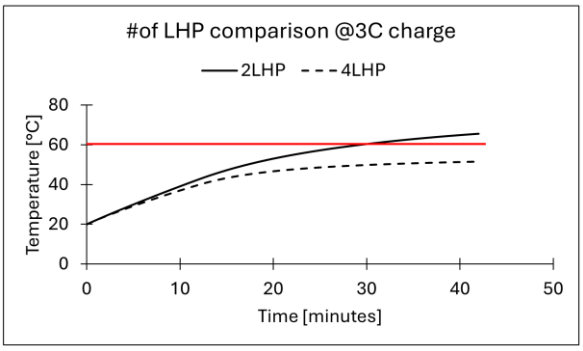

Figure 9. Comparison of the module cells average temperature during 3C charge followed by 1C cooldown when cooled by 2 or 4 LHPs.

LHP Temperature Results

Looking firstly at the LHP results presented in Figure 10, one can notice that indeed the condenser achieves full condensation, as the yellow line which represents the outlet temperature of the condenser, is in equilibrium with the ambient temperature in the 2C and 3C case (20 °C). In the 1C case, this happens only after the end of the charging phase, with the increased HTC given by the movement of the car. However, the condenser is properly sized as the final vapour quality if 0.07.

From Figure 10 however it is clear that despite the lower heating power of the 1C phase, the cell temperature keeps on increasing, without temperature drop. This does not pose a serious issue due to the timeframe of the phenomenon. However if several of these fast-charging followed by 1C driving cycles are happening one after the other in rapid succession, results indicate that the temperature would reach unwanted values. This suggests that the design following this feasibility study could be improved and optimized.

Cells Temperature Results

The cells temperature results shows that the proposed passive BTMS idea is feasible, as the temperature values are satisfactory. In more detail, the comparison graphs of Figure 11, demonstrates that the cell temperatures never reach the safety threshold of 60 °C, even after 3C fast charging (12 minutes). In fact, after the 3C fast charge and cooldown cycle, the maximum average cell temperature of the module is 51.6 °C, which is slightly above the acceptable threshold. However, it is important to point out that 3C fast charge is the state of the art, represented by the Porsche Taycan, which offers fast charge in 19 minutes; thus, this scenario would represent an improvement to the current EV charging situation.

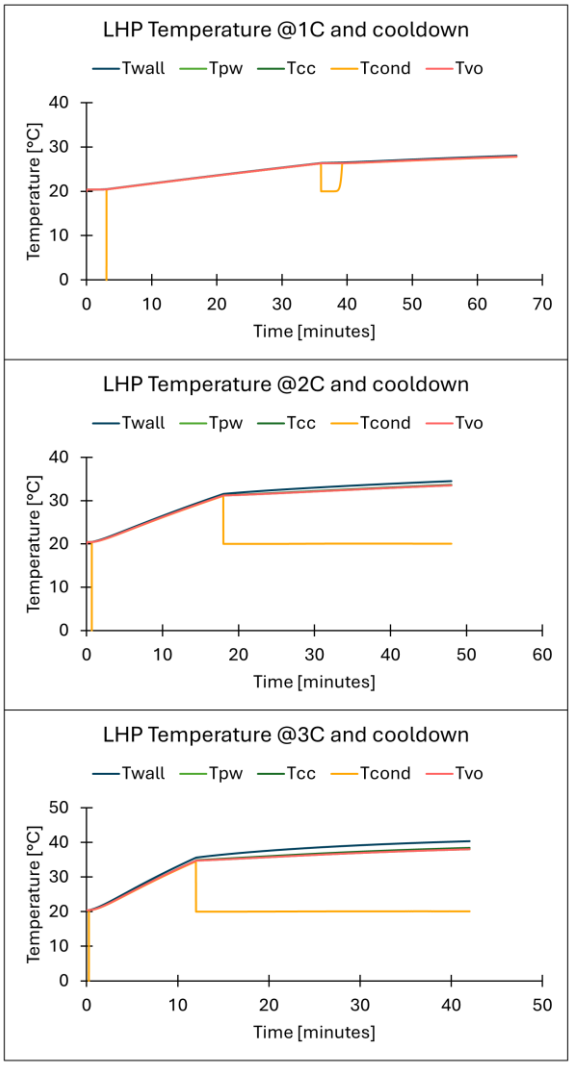

Figure 10. LHP nodes temperatures trends for 1C, 2C and 3C, showing full condensation at the condenser. Twall, Tpw, Tcc, Tcond and Tvo are the temperature of the wall, primary wick,

compensation chamber, condenser outlet and evaporator outlet, respectively.

Analyzing the 2C results, which correspond to an 18-minute fast charging scenario, reveals that cell temperatures consistently remain below the optimal threshold of 40°C, with a peak temperature of 39.3°C. This performance suggests the BTMS is well-suited for vehicle applications where charging times under 10 minutes are not essential (standard city cars, delivery vehicles, taxis).

Finally, for 1C, the maximum temperature reached by the cells was 27.5 °C, suggesting that a cooling system may be unnecessary under these conditions.

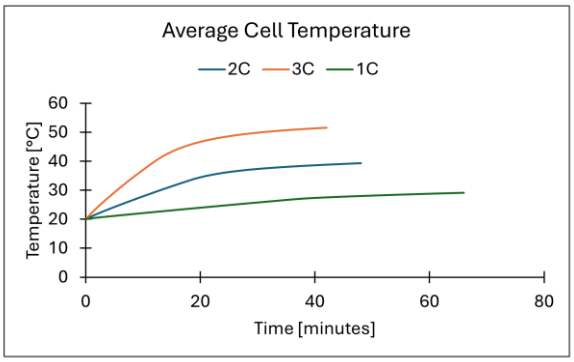

Figure 11. Average cell module temperature evolution at different fast charge cycles and cooldowns.

4. Conclusions

This work presents a feasibility study of a fully passive Battery Thermal Management System (BTMS) for Electric Vehicles (EV), utilizing Loop Heat Pipes (LHP) as a thermal vector, connecting the bottom of the battery pack with the underbody of the vehicle. In this way, aerodynamic cooling can be applied to the battery cells without spoiling the aerodynamic performance by introducing additional drag.

A two-tier open-source simulation procedure has been employed: firstly, utilizing CFD simulations on OpenFOAM to calculate the Heat Transfer Coefficient (HTC) at the underbody, due to the forced air convection created by the moving vehicle; secondly, an in-house generated and validated 1-D Lumper Parameter Model (LPM) predicted the thermal behavior of the cell and LHP assembly and helped to calculate the cell temperature evolution. Particular care was taken in ensuring that the condenser geometry would be suitable to achieve full condensation, at given HTCs.

The performance of this fully passive BTMS was evaluated over 1C, 2C, 3C charging cycles followed by a 30 minutes 1C driving section. The results can be summarized as follows:

- 2 LHPs are not able to maintain a 12-cell module under the 60 °C safety threshold, while with 4 LHPs the temperature requirements are met.
- The condenser was properly sized to achieve full condensation at the three charging cases.
- The proposed BTMS was able to contain the cell temperature inside the acceptable limits, even at challenging conditions such as 3C charging, with maximum temperature being 51.6 °C for 3C, 39.3 °C for 2C and 27.5 °C for 1C.

This work proved that this fully passive BTMS using LHPs and aerodynamic cooling is feasible and able to contain the battery cell temperatures in acceptable ranges.

5. Future Work

The next steps of this investigation revolve around expanding the simulated dataset, by including:

i) different driving cycles and C-rates;
ii) different working fluids;
iii) different LHP configurations;
iv) higher speeds and different ambient temperatures.

Following, the Authors will investigate the benefit of tailoring the LHP condenser design to the available HTCs, exploiting the fact that is higher towards the front of the vehicle.

The ultimate goal of this project would be to have coupled conjugated heat transfer simulations of a scenario where the LHP is physically embedded in the vehicle underbody and two-phase convection, conduction through solid and forced convection heat transfer mechanisms are all considered. With this in mind, the LPM model describing the cell-LHP thermal behaviour will be inserted into the OpenFOAM solver code to directly solve transient problems.

6. ACKNOWLEDGEMENTS

The Authors would like to thank the School of Architecture, Technology and Engineering at the University of Brighton for the financial support to attend this conference.

References

[1] International Energy Agency (IEA), Global EV Outlook 2020. , Paris, 2020.

[2] L. Noel, G. Zarazua de Rubens, B.K. Sovacool, and J. Kester, “Fear and loathing of electric vehicles: The reactionary rhetoric of range anxiety.,” Energy Research and Social Science. vol. 48, no. April 2018, pp. 96–107, 2019.

[3] P. Qin, M. Liao, D. Zhang, Y. Liu, J. Sun, and Q. Wang, “Experimental and numerical study on a novel hybrid battery thermal management system integrated forced-air convection and phase change material.,” Energy Conversion and Management. vol. 195, no. March, pp. 1371–1381, 2019.

[4] Q. Wang, P. Ping, X. Zhao, G. Chu, J. Sun, and C. Chen, “Thermal runaway caused fire and explosion of lithium ion battery.,” Journal of Power Sources. vol. 208, pp. 210–224, 2012.

[5] G. Zhao, X. Wang, M. Negnevitsky, and H. Zhang, “A review of air-cooling battery thermal management systems for electric and hybrid electric vehicles.,” Journal of Power Sources. vol. 501, no. April, p. 230001, 2021.

[6] A. Maiorino, C. Cilenti, F. Petruzziello, and C. Aprea, “A review on thermal management of battery packs for electric vehicles.,” Applied Thermal Engineering. vol. 238, p. 122035, 2024.

[7] M. Bernagozzi, A. Georgoulas, N. Miché, C. Rouaud, and M. Marengo, “Novel battery thermal management system for electric vehicles with a loop heat pipe and graphite sheet inserts.,” Applied Thermal Engineering. vol. 194, no. May, p. 2021.

[8] M. Bernagozzi, “Development and Characterisation of an Innovative Battery Thermal Management System for Electric Vehicles with Loop Heat Pipes and Graphite Sheets,” (2022).